UPDATING THE LIMIT EFFICIENCY OF SILICON SOLAR CELLS*

M. Wolf
University of Pennsylvania

The last recognized evaluation of the "limit-efficiency" and of design goals for silicon solar cells, based on realistic appearing material parameters and on an idealized device structure, was performed in 1970 under the auspices of the National Academy of Sciences (ref. 1). Since that time, a number of phenomena not recognized then have become reasonably well understood, and some device structuring approaches have evolved which permit "remedial designs" to gain high performance in albeit somewhat more complicated solar cell structures than envisioned earlier. These new circumstances warrant re-evaluation of both the idealized "limit efficiency" and of the design goals, the latter being values that can be expected to be approached in real, produceable devices.

An evaluation of the limit efficiency is suitably based on the simplest, most basic mathematical method that is appropriate for the conditions imposed by the cell model. In this connection, it is important to recognize that the "limit efficiency" has traditionally been evaluated for the idealized "one sun" case, which means no optical concentration and a normal irradiance of 1 kW m^{-2}, which has been obtained by a low-moisture, low-turbidity, direct-beam, air-mass 1 spectral distribution without addition of indirect radiation. For continuity and simplicity, this practice has been extended to this work. An evaluation of the "appropriateness" of approach has shown that the recalculation of the "limit efficiency", as essentially an upper limit, will be carried out with maximum clarity and fully adequate accuracy by application of the existing basic analytical model of a solar cell (ref. 2) to a simple, idealized solar cell structure. From this limit efficiency, a first set of "design goals" can be derived by application of "experience factors", as done here. However, the design calculations can be improved by more sophisticated modeling, which will permit the close evaluation of the relative merits of various realizable structure design options. Following a stepped procedure, in moving from the idealized structure to one more closely resembling a real current or projected design and in applying more sophisticated analysis methods, will have dual benefits: It permits determining the influence on performance of each part of the real solar cell structure relative to the idealized structure; and it permits an evaluation of the relative accuracies obtainable by applying exact analytical methods to approximate structure or operating mechanism models in contrast to applying numerical methods to more closely representative models.

This publication deals only with the limit efficiency obtainable by application of the base analytical method to the simplest idealized solar cell

---

*This work was performed in connection with the activities of the Advisory Group on High Performance, Low-Cost Solar Cells to the DOE/JPL LSA Program, and was partially supported by the U.S. Department of Energy through the Jet Propulsion Laboratory under contract No. KM 68903.

structure. It contains a description of the methodology, of the solar cell structure, of the selection of the material parameters used in the evaluation, and a discussion of the results, including a new set of design goals derived from the limit efficiency. Further publications, in preparation, will extend, in a simple way, the one-dimensional analytical method which is accurately applicable at low level injection to any quasi-neutral region with constant parameters in the device, to general multilayer structures, and apply it to solar cells with at least 2 to 3 layers in each of the two main regions of the device, closely approximating currently realizable structures.

DIFFERENCES TO PRIOR EVALUATIONS OF SOLAR CELL LIMIT EFFICIENCY

A significant number of endeavors have previously been undertaken at determining a "limit efficiency" of solar cells in general, and in particular of silicon solar cells. These endeavours fall essentially into two groups: In the first, the researchers have tried to establish an "absolute theoretical efficiency" based on the application of basic physical principles only, without introduction of structure or material parameters. Some of these approaches were based primarily on the laws of thermodynamics (ref. 3). The larger number of endeavours fall into the second group, having been based on contemporary semiconductor device analysis methods, applied to a somewhat idealized device structure, and using, at the time, realistic appearing material properties. In this second group, the structures were idealized in so far as known, technology-limited effects were extrapolated to levels which appeared to be achieveable in the future, or to the 100% performance level, where the losses resulting from such effects were already rather small. Following the current penchant for abbreviations, this second group might suitably be classified as ReMPIDS modeling, with the abbreviation standing for "realistic material parameters/idealized device structure."

There are clearly three preceding generations of the ReMPIDS approach discernible, so that the current undertaking would represent the fourth generation. The preceding generations date to the 1953-55 period (ref. 4), the 1958-61 periof (ref. 5), and to 1970 (ref. 1). The 1970 model, developed for a committee commissioned by the National Academy of Sciences, was concerned primarily with illuminating the technologically feasible appearing methods for improving the efficiency of the silicon solar cells beyond that at which they had stagnated for a number of years.

The key results of this 1970 analysis included the potential collection efficiency increase from the contemporary level of 72% to about 88% by improving the short-wavelength response of the device through thickness reduction of the diffused region and a modest decrease of the "effective surface recombination velocity" at the front surface of the cell, and additionally through a moderate increase of the diffusion length in the base region, as well as a small reduction in the reflectance of the front surface. A larger efficiency improvement was expected from an increase in the open circuit voltage and the curve factor. Based on applying Shockley's diffusion theory for PN junction characteristics and the Shockley-Read theory of recombination, this improvement was predicted to be achieved primarily by reducing the resistivity of the base region with maintenance of a reasonable minority carrier saturation lifetime at these lower resistivities. The following assumptions had been

made in that analysis, which were characteristic of the understanding of that time: (a) the surface recombination velocity approaches infinity under the ohmic contacts, and is very high and only moderately influenceable on the open front surface; (b) the onset of Auger recombination and of band-gap narrowing at very high impurity levels was not recognized; (c) wide-base diode analysis was applied since it appeared valid on the basis of contemporary diffusion length to or beyond the base width had not been recognized which might have necessitated the application of appropriate correction factors for narrow base widths in these measurements.

The improvements in the collection efficiency predicted by the 1970 ReMPIDS modeling effort, were achieved rather quickly and amazingly close to the predicted value (ref. 6). However, the long wavelength collection improvement and the reflectance reduction were achieved essentially by a clever workaround, namely by texturing the front surface of the solar cell (ref. 7). In addition, considerable efforts have been spent to achieve the predicted voltage and curve factor improvements, but open circuit voltages exceeding approximately 0.62 Volt at 28°C could not be obtained. Consequently, numerous speculations for the potential causes of this apparent "open circuit voltage limitation" were advanced, which gradually narrowed down to the most likely effects of Auger recombination (ref. 8) and bandgap narrowing (ref. 9). (Table I)

In addition to the introduction of the "textured" solar cell surface, an optical internally reflecting back contact has also been introduced in recent years (ref. 10). While the former causes the photons to transit the solar cell bulk material, before absorption, under oblique angles rather than normal, in normally incident light, the latter provides a second chance for absorption, with charge carrier generation, for those photons which would otherwise have been absorbed, without carrier generation, at the back contact surface. Thus, both measures serve to create the effect, for the absorption of photons, of the existence of a thicker wafer than is actually used.

In parallel to these experimental efforts, the understanding of the cell operating mechanisms also advanced further. In 1972, it had already been shown that a drift field in a part of the base region can be used to considerably reduce the influence on the collection efficiency normally exerted by the high surface recombination velocity from the back contact (ref. 11). Simultaneously, it was recognized that with the contemporary tendency to increasing diffusion lengths and decreasing base region thicknesses, the transition to intermediate width and narrow width base regions was occurring. Consequently, the diode saturation current should be expressed as

$$j_o = j_{o,\infty} \cdot (GF)$$

where $j_{o,\infty}$ is the commonly used saturation current for the wide base diode, and (GF) is a dimensionless "geometry factor", which describes the influence of the physical configuration (ref. 12, 11) (Fig. 1). It thus was shown, that the dark diode saturation current in intermediate and narrow base diodes can be considerably larger or smaller than the corresponding saturation current in the wide base diode, depending on the magnitude of the surface recombination velocity (ref. 11). About the same time, interest started to steadily grow in the application of a drift field in a narrow part of the base region near the back contact surface which gradually led to the coining of the name "Back

Surface Field" (BSF) solar cell (ref. 13). A great deal of speculation has developed about the actual influence of such a drift field on the carrier transport in the base region which is still not fully resolved. Also, application of the narrow-base corrections in the measurements of diffusion length in solar cells has started, and amazingly long diffusion lengths were found (ref. 14). But despite the gradually growing acceptance of these new recognitions, they have not been applied to a reevaluation of the limit efficiency of the silicon solar cell.

The current application of the ReMPIDS model thus differs from the last prior one in the following details: (a) the availability of high minority carrier lifetime material, with consequently long diffusion lengths; (b) the applicability of intermediate width or narrow-base diode theory, partially in consequence of point a); (c) the surface recombination velocity has no longer to be reckoned with as a nature-given, essentially unalterable effect since both theoretical and experimental efforts have indicated that the influence of surface recombination velocity can be greatly reduced by applying drift field regions, inversion layers, or wide band-gap windows; (d) thinner base regions can be advantageously used by application of a textured cell front surface and an optical internally reflecting back contact; and (e) the application of very low resistivity material entails the introduction of Auger recombination, bandgap narrowing, and possibly other performance degrading effects.

As an outcome of point (a) above, "realistic material parameters" should now include the use of minority carrier lifetime values as obtained on the best recently available silicon. These values are approximately an order of magnitude higher than those used previously. Also, in consequence of point (c) above, the "idealized device structure" can appropriately include the use of zero surface recombination velocity on both the front and back surfaces of the solar cell.

THE ANALYTICAL MODEL

The analytical model used is a transport equation for minority carriers derived from the Shockley equations (ref. 15) which contain descriptions of the continuity of charge carrier flow, including generation and recombination, for both electrons and holes, and of the electrical current based on diffusion and on drift of charge carriers, again for holes and electrons. The generation term in this transport equation is based on charge carrier pair generation by photon absorption, with a wavelength dependent absorption coefficient according to the specific semiconductor used, and to the operating temperature. The photon incidence is assumed to be uniform over the light-exposed surface of the solar cell. Also, the geometry of the device is taken as plane and parallel to the front surface, and the two dimensions of these planes are assumed to be very large compared to the diffusion length of the minority carriers, so that surface effects at the edges of the device can be neglected. These two assumptions, together with a third one stipulating the uniformity of all relevant material parameters in the planes parallel to the front surface, permit the transport equation be written and solved in one-dimensional form. In addition to this condition of "planar uniformity", the condition of "low level injection" is imposed to obtain independence of the minority carrier lifetime from carrier concentration, and to avoid the requirement for coupled solution with a second

transport equation describing the majority carrier flow. The third key condition imposed is that of maintenance of "space charge neutrality" which eliminates the need for using the Poisson equation as a further coupled differential equation.

With these three conditions, and for the steady state case of interest here, the transport equation becomes an inhomogeneous one-dimensional, linear, second order differential equation, which can be analytically solved for certain cases. Imposing the low level injection condition is instrumental in providing linearity of the differential equation, and maintaining the linearity of the transport equation permits the superposition of the different solutions arising from various forcing functions. Such forcing functions describe, for instance, minority carrier injection across the pn junction due to forward bias, or the generation of minority carriers from photons within a given wavelength band of the spectral distribution of the light source. This latter feature provides the possibility of obtaining separate solutions, and thus individual light generated current contributions, for each individual spectral range, and the superposition of these solutions over the whole spectral distribution of the source, to obtain the total light generated current. Similarly, separate solutions of the transport equation, obtained for the two major regions of the solar cells, can be superimposed both for the light generated current and the diffusion current injected across the PN-junction under forward bias condition. The two major regions of the device are the front region, which is defined as the region between the light exposed front surface of the device and the boundary surface between the depletion region of the PN junction and this layer; and the base region, which is the region between the back surface of the cell and the boundary surface between the depletion region and this base layer. The third major region is the depletion region of the PN junction, which also contributes light generated current. For the idealized device structure, the assumption has been made that recombination does not take place in this depletion region, resulting in 100% collection efficiency for this region.

Through the additional assumption of constancy in the direction of minority carrier mobility and lifetime and, where present, the drift field, throughout a region of the semi-conductor device for which a solution of the differential equation is to be found, the transport equation becomes a differential equation with constant coefficients, for which an analytical solution can be readily found (ref. 16). In most cases where the conditions and assumptions outlined here are not fulfilled, only numerical methods can be applied to the solution of the transport equation or the coupled system of equations. For the idealized device structure treated here, the analytical solution is fully appropriate. However, for most real silicon solar cell structures, and under many of their applications, the analytical method also provides a very good approximation, as long as it is realized that it cannot yield information for certain effects which may be interesting for study.

The general solution of the transport equation is subjected to the appropriate boundary conditions which, in this particular application, include zero surface recombination velocity at both the front and the back surfaces. The PN junction itself is modeled according to Shockley's diffusion theory which means that the injection currents are based exclusively on recombination

within the bulk and at the surfaces of the neutral regions. It has been shown in carefully prepared solar cells that the recombination current from the depletion region can be made negligibly small in the part of the I-V characteristic near the maximum power point, which is the only part of interest for the establishment of the limit conversion efficiency. The diffusion or injection current is determined for both regions according to the impurity concentrations chosen for the individual cell structure. A single-sided injection model is not used. Also, the diffusion currents are obtained for the actual thicknesses of the two regions chosen for the cell structure, so that their determination is not limited by either wide base or narrow base assumptions. Although recombination in the depletion region is neglected, its width is not assumed to be zero, but is calculated from the linear graded junction model. The diffusion currents are then determined for the actual dimensions of the neutral regions.

The computations of the light generated currents have been based on the Airmass 1 sunlight spectrum. Its spectral distribution and irradiance have been derived from the Airmass 0 spectral distribution, with an irradiance of 135.3 mW cm^{-2}, according to the NASA/ASTM Standard (Ref. 17). This derivation has been based on the computation of the atmospheric absorption using the Bouguer relationship (Ref. 18), by assuming an ozone content of 2.5 mm, a precipitable water content of 10 mm, and a dust content of the atmosphere of 300 particles per cubic meter. A total direct Airmass 1 irradiance of 99.3 mW cm^{-2} is thus obtained, and no indirect radiation has been added.

The solutions of the transport equation under the appropriate boundary conditions are available in a computer program which steps, in 50 nm wavelength increments, through the whole Airmass 1 solar spectrum to determine the total light generated current contributions from each of the three regions of the solar cell, as well as the total for the cell. Similarly, applying the corresponding solution of the transport equation without the generation term provides the diffusion current from the front and the base regions for zero bias condition. Having obtained the total light generated current and the diffusion current, the entire current-voltage characteristic for the idealized-structure solar cell is determined. In an iteration procedure, the maximum power point of this current-voltage characteristic is then found, using a series resistance value entered as a parameter into the computation. For the current evaluations of an idealized model, this series resistance is assumed to be zero.

It may be noted that for the values of impurity concentration assumed for the front and the base regions, the condition of low level injection is maintained for the light generated current in any part of the cell up to light intensities which would correspond to moderate optical concentration ratios, i.e. ratios in the 10 to 100 range.

A violation of the low level injection condition can arise, however, from the diffusion current in certain device configurations (Ref. 19). This situation can occur, for instance, in regions adjacent to the depletion region, which are very narrow compared to a diffusion length, and out of which very little minority carrier flow occurs, as would be the case from layers with low surface recombination velocity. Also, large diffusion currents are needed primarily at or near the open circuit condition, at which the diffusion current has to be equal

and opposite to the light generated current. This phenomenon is illustrated in Fig. 2, simplified by considering all light generated current to be originating from the base region, and all diffusion current flowing into the base region. Figure 2 shows that the current equality requires

$$\left.\frac{dn_L}{dx}\right|_{x=x_{j,B}} = -\left.\frac{dn_d}{dx}\right|_{x=x_{j,B}}$$

assuming that both currents are principally based, near the depletion region, on carrier diffusion. The subscripts "L" and "d" indicate minority carriers resulting from light generation and injection across the depletion region, respectively. $x_{j,B}$ denotes the depletion region boundary on the base side. It is thus the minority carrier density gradients, and not the densities themselves, that have to be equal. In fact, the diffusion current equals the total recombination in the base region, postulating negligible minority carrier outflow. But the recombination rate U is proportional to the minority carrier density, in low level condition. Thus, if the minority carrier lifetime (τ_n) is large, a high minority carrier density is needed to achieve a given recombination rate. This is commonly expressed in the "charge control model"

$$q \int_{x_{j,B}}^{x_{B,1}} U dx = \frac{q}{\tau_n} \int_{x_{j,B}}^{x_{B,1}} (n_d - n_o)\, dx = \frac{Q_n}{\tau_n}$$

where τ_n is kept constant in accordance with the low level condition. Q_n is the total charge stored in the base region by minority carriers n_d injected across the depletion region, n_o being the equilibrium minority carrier concentration. Thus n_d can be much larger than n_L, and can begin to violate the "low level" condition, or even approach the "high level" condition, long before n_L leaves the low level situation.

Here, however, only the determination of the limit efficiency is of concern, which entails a performance evaluation at or near the maximum power point. At this point, the needed diffusion current density is approximately an order of magnitude smaller than that for the open circuit condition. Thus, the low level injection condition in this part of the I-V characteristic is still maintained in nearly all practical cases of concern here.

THE "REALISTIC MATERIAL PARAMETERS"

The evaluation of the limit solar cell performance has been performed for a

range of resistivities in the base and front regions of the cell, respectively. In most cases, the front region resistivity has been made at least one order of magnitude lower than the resistivity of the base region. However, to avoid complications encountered through the onset of bandgap narrowing, through a severe influence of Auger recombination, or other possible very low resistivity effects, the highest impurity concentration used in these calculations has been $2x10^{18}$ cm^{-3}.

The key material parameters needed for the calculations are the minority carrier mobility and the minority carrier lifetime. For the minority carrier mobility, relatively recent experimental data have been used (Ref. 20). For the minority carrier lifetime, a set of values at three different resistivities, was chosen which is representative of experimental values repeatedly found in the best available silicon of the respective resistivities. (See the 3 points shown in Fig. 3) These minority carrier lifetimes are therefore thought to be fully within the capability of today's silicon material technology and should, once appropriate attention is paid to this aspect, be produceable in quantity at acceptable prices for solar cell manufacture. These lifetime values are applicable in both n-type and p-type material. Lifetime values at resistivities other than the three given points were obtained by interpolation and extrapolation using Shockley-Read recombination theory and Auger recombination. (Ref. 21) (Fig. 3) The data of Fischer and Pschunder (Ref. 8) show the availability of 1 ms lifetimes already at a 1 Ω resistivity, and indicate a very high saturation lifetime based on a small concentration of deep levels, so that no influence of doping concentration occurs, outside of Auger recombination.

THE IDEALIZED SOLAR CELL STRUCTURE

As was outlined in the section on the "analytical model", the basic solar cell structure is assumed to be plane parallel, and extending, in the lateral dimensions, far in comparison to the minority carrier diffusion length. The basic cell structure is assumed to consist of three regions: the front region, the transition region, and the base region, arranged in this order counting from the front surface of the cell. As was mentioned, the width of the transition region is computed using the linear graded junction model. While recombination in this region is assumed to be zero, the collection efficiency of this region is assumed to be 100%. The front and the base regions of the cell have been assumed to have constant material parameters throughout, and to be free of any electrostatic field.

As an extrapolation from current technology capabilities, the surface recombination velocities at the front and the back surfaces of the cell have been assumed to be zero. This assumption can be interpreted in a different way: There could be an idealized layer, in front of the front region, of such properties that it transmits 100% of the incoming photons into the solar cell, but transforms the electronic properties of the open surface so that, at the interface of this additional front layer with the active front layer of the cell, a boundary exists into which no minority carrier current flows. Simultaneously, the interface and the layer itself shall have no resistance to majority carrier current flow. Such a layer might be a "window layer" of a wide band gap ma-

terial, similar to the usage in the $Ga_xAl_{1-x}As/GaAs$ solar cells, or a layer incorporating a "high low junction", or an inversion layer. A similar idealized layer could be assumed to be interspersed between the real back surface of the cell and the base region. This layer would have the same electronic properties as the "idealized window layer", but it needs not to be transparent to photons. This layer would, however, have to effect a suitable transformation from the electronic properties of an ohmic contact which normally has a much higher surface recombination velocity than an open surface should have, and which generally covers the entire back surface of the cell.

Two additional features have been incorporated into the solar cell structure. The first is the assumption of a textured front surface, which causes the photons to penetrate under oblique angles into the solar cell structure. This effect is modeled in an idealized manner by assuming all photons to move inside the solar cell at the same penetration angle, which could be visualized as the average of all actual penetration angles. This average angle has been chosen here as 45° from the normal to the solar cell planes, a value which should be close to that resulting, in normal incidence, from the surface structure usually obtained in the common texture etching processes. (Ref. 7)

The second feature is the existence of an optically reflecting surface at the rear of the base region. The existence of this surface feature permits photons which penetrate all the way through the front, depletion, and base regions of the cell, to be reflected forward and have a second chance for absorption and charge carrier generation. For the idealized cell structure, a reflectance of 1.0 has been assumed for the back surface. Together with the textured front surface, the reflecting back surface permits the construction of a thinner solar cell with the same absorption characteristic and a possibly even higher collection efficiency as would otherwise be obtained in a thicker cell structure.

For a sensitivity analysis, the cell configuration which appeared readily practically realizable and gave one of the highest efficiencies, was recomputed with two different values of surface recombination velocity: 10 cm s^{-1} and 100 cm s^{-1}.

RESULTS OF THE COMPUTATIONS

Around a hundred computations were made with different material parameters and device structures to obtain: a) the absolute maximum, or limit efficiency; b) the optimum efficiency obtainable with certain material combinations; and c) the sensitivity to changes in various structure parameters. Only the key results are summarized in Table II and in Figures 4 to 8. These results lead to the following observations:

1. The idealized limit efficiency is still about 25%, the highest value found was 25.13%.

2. There is still a tendency towards higher efficiency at the lower resistivities. (Fig. 4)

3. Very low resistivities, involving impurity concentrations above 10^{18} cm^{-3}, are not needed for achieving the limit efficiency.

4. In consequence of point 3, high doping effects, including degeneracy, serious influence of Auger recombination, band-gap narrowing, etc., can be avoided.

5. The limit efficiency value obtained is, however, determined by the onset of Auger recombination which depresses this efficiency slightly.

6. There is a very wide range of impurity concentrations at which idealized efficiencies above 23.5% are obtainable.

7. Idealized efficiencies above 23.5% are obtained at total wafer thicknesses of 25 to 200 μm, and at junction depths of 2 to 10 μm. This means rather thin cells and large junction depths, in contrast to earlier thinking.

8. The higher the impurity concentration chosen, the smaller the junction depth and the total cell thickness have to be. The limit efficiency has been obtained at a total cell thickness of only 50 μm, with junction depths of 2 to 6 μm.

9. In all cases of high efficiency, the region thickness is small compared to the diffusion length within it. The limit efficiency, however, has been obtained in a case where this statement is only marginally valid.

10. The peak efficiency values are obtained in a design trade-off between collection efficiency and voltage (Fig. 5 to 6). As the cell thickness is decreased, the collection efficiency decreases due to reduced photon absorption, while the voltage increases, based on the reduction of the diode saturation current resulting from the decrease of the form factor with decreasing thickness at low surface recombination velocity.

11. The best efficiencies are obtained with equal impurity concentrations in the front and base regions of the cell. Thus, there is principally no need for an "emitter" in the front region, except that higher doping can help to reduce series resistance.

12. Both the textured surface and the optical internally reflecting back surface are important for obtaining high efficiencies in thin cells, and small cell thickness, in turn, is needed to approach the high conversion efficiency values shown here.

13. The optimum efficiencies are obtained over a rather broad range of material and structure parameters, and the sensitivities to the variation of these parameters are generally small (Fig. 7 to 8).

14. Since greater cell thicknesses and wider ranges of junction depth are available at lower impurity concentrations, these cells will probably find preference for practical reasons (Fig. 4).

15. The sensitivity of the efficiency to low values of surface recombination velocity is also not great (Table II, lines 14 to 15, compared to line 4).

DISCUSSION OF RESULTS

The assumption of low or zero surface recombination velocity at the surfaces, combined with oblique penetration of the photons into the solar cell as results from surface texturing, and with optical internal reflection at the back surface leads to a new approach to solar cell design and optimization. While the earlier thinking was based on obtaining high voltages, and consequently high conversion efficiency, by application of very high impurity concentrations to yield a low diode saturation current, the new approach pursues the same goal of low saturation current by using front and back regions of the solar cell which both are narrow compared to the respective diffusion lengths. Thus, the severe limitations imposed by heavy doping effects are avoided, and high efficiencies still are obtainable. However, this cell design involves a trade-off between the collection efficiency and the cell voltages. This trade-off can not be optimized without the oblique penetration of the photons and the internal optical reflection. In fact, in the highest efficiency case found, in which the base region thickness happens to approach the diffusion length (Table II, Line 11), Fig. 4 shows clearly that a further increase of the base region thickness results in reduced light generated current, as fewer of the minority carriers are collected which were generated from photons which had been internally reflected at the back surface. This case clearly illuminates the importance of the optical internal reflection at the back surface in very thin cells.

Table I repeats a set of numbers which were derived in 1970 as design "goals" for the key performance parameters of silicon solar cells in Airmass 0 sunlight, together with the actual data of contemporary cells and improved cells developed since then. The insights gained with the analysis of a new limit efficiency, described here, indicates that a preliminary reevaluation of the design goals would also be appropriate. The results of such a reevaluation are summarized in Table III, using the data on the idealized, 100 μm thick cell with 4 μm thick front layer of 5.10^{17} cm^{-3} n-type impurity concentration, while the p-type base region contains 5.10^{16} cm^{-3} impurities. These data determine the collection efficiency, the open circuit voltage, and the curve factor. The other parameters correspond essentially to current experience factors on the better cells. The preliminary goal thus found for silicon solar cells is 22% conversion efficiency in Airmass 1, unconcentrated sunlight at 28°C. This goal needs refinement through further investigations to determine to what degree the idealized cell structure and its performance can be approached in real solar cells.

CONCLUSIONS

The new computations on idealized solar cell structures have shown that there is a second "theoretical approach" to obtaining high open circuit and maximum power point voltages, after the first one, relying on high impurity concentrations in the base and front regions of the cell, has been found in-

feasible. This second approach involves the "narrow region" design for both the front and back regions of the solar cell, and relies heavily on low effective surface recombination velocities front and back, as well as a textured front surface and an optical internally reflecting back surface. In fact, using this design, the undesirable effects of high doping can be completely avoided. The idealized limit efficiency of the solar cell, the validity of which had become doubtful as a result of the recent realization of the impacts of high doping effects, is thus reestablished at its earlier value near 25%. The new cell design requires a rather thin cell, in the 50 to 150 μm range, with a thick front region in comparison to contemporary designs. Of paramount importance, however, is obtaining low effective surface recombination velocities both at the front and back surfaces of the cell. These may be approached by the use of drift field, inversion, or window layers. Further investigations in progress are aimed at exploring the degree to which the assumptions made, particularly that of extremely low surface recombination velocity, can be expected to be approached in real solar cell structures. Early results from these investigations indicate, that an amazingly close approach to the performance of the idealized solar cell structure may be possible in real solar cells.

REFERENCES

1. Wolf, M., "A New Look at Silicon Solar Cell Performance", Rec. 8th IEEE Photovoltaic Spec. Conf., IEEE Cat. #70C32ED, pp. 360-371, Aug. 1970; also in: "Solar Cells, Outlook for Improved Efficiency", Nat'l Acad. Sciences, 1972.

2. Wolf, M., "Limitations and Possibilities for the Improvement of Photovoltaic Solar Energy Converters", Proc. IRE 48, pp. 1246-1263, (1960).

   Wolf, M., "The Solar Cell Design Handbook", Rec. 9th IEEE Photovoltaic Spec. Conf., pp. 53-60, IEEE Cat. No. 72 CHO 613-0-ED, (1972).

3. Muser, H.A., Z. Phys. 148, 380 (1957).

   Rose, A., "Photovoltaic Effect Derived from the Carnot Cycle," J. Appl. Phys. 31, 1640 (1960).

   Shockley, W., and Queisser, H.J., "Detailed Balance Limit of Efficiency of pn Junction Solar Cells", J. Appl. Phys. 32, 510-519 (1961).

4. Prince, M.B., "Silicon Solar Energy Converters", J. Appl. Phys. 26, 534-540 (1956).

   Loferski, J.J., "Theoretical Considerations Governing the Choice of Optimum Semiconductor...". J. Appl. Phys. 27, 777-784 (1956).

5. Wolf, M., see ref. 2, item 1.

   Kleinman, D.A., "Considerations on the Solar Cell", Bell. Syst. Tech. J. 40, pp. 85-115, (January 1961).

Wysocki, J.J., and Rappaport, P., "Effect of Temperature on Photovoltaic Solar Energy Converters", J. Appl. Phys. 31, 571-578 (1960).

6. Wolf, M., "Outlook for Si Photovoltaic Devices for Terrestrial Solar-Energy Utilization", J. Vac. Sci. Technol. 12, pp. 984-999, (1975).

7. Haynos, J., et. a., "The COMSAT Non-Reflective Silicon Solar Cell: A Second Generation Improved Cell," Photovoltaic Power Generation, pp. 487-500, Proc. Int'l Conf. Photovoltaic Power Conversion, (DGLR), Kiln (1974).

8. Fischer, H., and Pschunder, W., "Impact of Material and Junction Properties on Silicon Solar Cell Efficiencies", Record 11th IEEE Photovoltaic Spec. Conf., IEEE Cat. No. 75 CHO 948-OED, pp. 25-31 (1975).

9. Godlewski, M.P., et. al., "Effects on High Doping Levels on Silicon Solar Cell Performance", ibid., 32-35 (1975).

   Lindholm, F.A., et. al., "Fundamental Limitations Imposed by High Doping on the Performance of PN Junction Silicon Solar Cells", ibid., pp. 3-12.

10. Ralph, E.L., private communications.

11. Wolf, M., see ref. 2, item 2.

12. McKelvey, J.P., "Solid State and Semiconductor Physics", pp. 420-423, Harper and Row, N.Y. (1966).

13. Mandelkorn, J., and Lamneck, H. Jr., "Simplified Fabrication of Back Surface Electric Field Silicon Cells", Rec. 9th IEEE Photovoltaic Spec. Conf., IEEE Cat. No. 72 CHO 613-0-ED, (1972).

14. Fossum, J.G., and Burgess, E.L., "High Efficiency p^+-n-n^+ Back-Surface-Field Silicon Solar Cells", Appl. Phys. Lett. 33(3), pp. 238-240 (1978).

15. Shockley, W., Bell Syst. Tech. J., 28, pp. 435- (1949).

   Shockley, W., "Electrons and Holes in Semiconductors", Van Nostrand, Princeton, N.J. (1950).

16. Wolf, M., "Drift Fields in Photovoltaic Solar Energy Converter Cells", Proc. IRE 51, pp. 674-693, (1963).

17. Thekaekara, M.P., Solar Energy 14, pp. 109-127 (1973). Anon, 1974 Annual Book of ASTM Standards, Part 41, E490-73a, pp. 609-615, ASTM, Philadelphia, PA. (1974).

18. Moon, P., J. Franklin Inst. 230, pp. 583-617 (1940).

19. Fossum, J.G., et. al., "Development of High-Efficiency P^+NN^+ Back-Surface-Field Silicon Solar Cells", Rec. 13th IEEE Photovoltaic Spec. Conf., IEEE Cat. No. 78CH1319-3 pp. 1294-1299, (1978).

20. Wolf, H.F., "Semiconductors", p. 276, Wiley-Interscience, NY, 1971.

21. Shockley, W., and Read, W.T., Phys. Rev. 87, pp. 835 (1952).

TABLE I. - PERFORMANCE STATUS OF CURRENT SILICON SOLAR CELLS AND IMPROVEMENT GOALS

Attribute	Goal	Efficiency contribution (1-Loss): 1970 Comm'l. Cell	"Violet" Cell	"Black" Cell	Output values	Goal	Black Cell	
Basic Losses	0.45	0.45	0.45	0.45	Light generated current	63.0	63.0	mW cm^{-2}
Collect. Eff'y	0.88	0.71	0.79	0.88		49.0	49.0	mA cm^{-2}
Reflection	0.97	0.905	0.951	0.97		47.5	47.7	mA cm^{-2}
Grid Line Cover	0.96	0.96	0.95	0.95		45.5	45.4	mA cm^{-2}
Voltage Factor	0.61(?)	0.522	0.535	0.531		0.675	0.591	V
Curve Factor	0.86	0.82	0.825	0.822	Power	26.3	22.1	mW cm^{-2}
Add'l Curve Fact.	1.0	0.91	1.0	0.99		26.3	21.8	mW cm^{-2}
Series Resistance	0.97	0.96	0.985	0.984		25.6	21.4	mW cm^{-2}
Efficiency (AMO)	0.19	0.104	0.14	0.153				

TABLE II. - SUMMARY OF RESULTS OF COMPUTATIONS

Line	Wafer Thickness	Region 1 (Base), p-type					Region 2 (Front), n-type						Region 3 (Transition)		Total Cell			
	d μm	Impurity Conc. N_A cm^{-3}	Diffusion Length L_n μm	Surf. Recomb Veloc. S_1 cm s^{-1}	Light Gen'd. Curr't $j_L(1)$ mAcm^{-2}	Saturation Curr't $j_o(1)$ A cm^{-2}	Impurity Conc. N_D cm^{-3}	Nom'l Thickness x_j μm	Diffusion Length L_p μm	Surf. Recomb Veloc. s_2 cms^{-1}	Light Gen'd Curr't $j_L(2)$ mAcm^{-2}	Saturation Curr't $j_o(2)$ Acm^{-2}	Nom'l Thickness Δx_j μm	Light Gen'd Curr't $j_L(3)$ mAcm^{-2}	Light Gen'd Curr't j_L mAcm^{-2}	Open Circ't Volt. V_{oc} V	Curve Factor (CF) --	Conv. Effic'y. η %
1	150	7.10^{14}	1670	0	14.1	3E-13	5.10^{17}	4	60.3	0	26.0	1E-15	1.18	1.8	41.9	0.665	0.84	23.6
2	100	5.10^{15}	604		9.1	1E-13	5.10^{16}	10	135		31.8	7E-15	0.24	0.08	41.1	0.681		
3		5.10^{16}	225		10.2	7E-14		8	135		30.5	6E-15	0.20	0.15	40.8	0.700	0.85	24.3
4					14.5		5.10^{17}	4	60.3		26.0	1E-15	0.15	0.27		0.701		
5	200				14.9	1E-13									41.1	0.687	0.84	24.0
6	50				13.2	4E-14									39.5	0.717	0.85	24.2
7					8.8	3E-14		8			30.5	2E-15		0.11	39.4	0.719		
8					23.0	4E-14		1			15.5	3E-16		1.0	39.5	0.716		
9	150				24.5	1E-13					15.4				41.0	0.692	0.84	24.1
10					10.6			8			30.3	2E-15						
11	50	5.10^{17}	97.6		13.0	1E-14		4			26.0	1E-15	0.06	0.11	39.1	0.748	0.85	25.12
12					18.0		2.10^{18}	2	21.8		20.7	9E-16	0.05	0.19	38.9	0.747		25.0
13	25	2.10^{18}	34.5		12.7	6E-15		3			23.8	1E-15	0.04	0.10	36.6	0.756		23.8
14	100	5.10^{16}	226	10	14.5	7E-14	5.10^{17}	4	60.3	10	26.0	1E-15	0.15	0.27	40.7	0.700		24.3
15				100	14.3	9E-14				100	25.8	4E-15			40.4	0.69	0.84	23.8

TABLE III. - PRELIMINARY 1979 SILICON SOLAR CELL DESIGN GOALS

Attribute	Performance Factors: Airmass 0, 1970*	Performance Factors: Airmass 0, 1979 Prelim.	Performance Factors: Airmass 1, 1979 Prelim.	Output Values: Airmass 0, 1970*	Output Values: Airmass 0, 1979 Prelim.	Output Values: Airmass 1, 1979 Prelim.	
				59.5	59.5	49.6	$mW\ cm^{-2}$
Basic Losses	0.44	0.44	0.50	53.3	53.3	44.3	$mA\ cm^{-2}$
Collection Efficiency	0.88	0.93	0.93	46.9	49.4	41.0	$mA\ cm^{-2}$
Reflection	0.97	0.97	0.97	45.4	47.9	39.8	$mA\ cm^{-2}$
Grid Line Coverage	0.96	0.95	0.95	43.5	45.5	37.8	$mA\ cm^{-2}$
Voltage Factor	0.61	0.63	0.63	0.675	0.706	0.701	V
Curve Factor	0.86	0.85	0.85	25.2	27.3	22.4	$mW\ cm^{-2}$
Add'l Curve Factor	1.00	1.00	1.00	25.2	27.3	22.4	$mW\ cm^{-2}$
Series Resistance	0.97	0.985	0.985	24.5	26.8	22.1	$mW\ cm^{-2}$
Efficiency	0.182	0.198	0.221				

*Corrected from previously used Johnson spectrum to the current NASA/ASTM Airmass 0 absolute spectral distribution

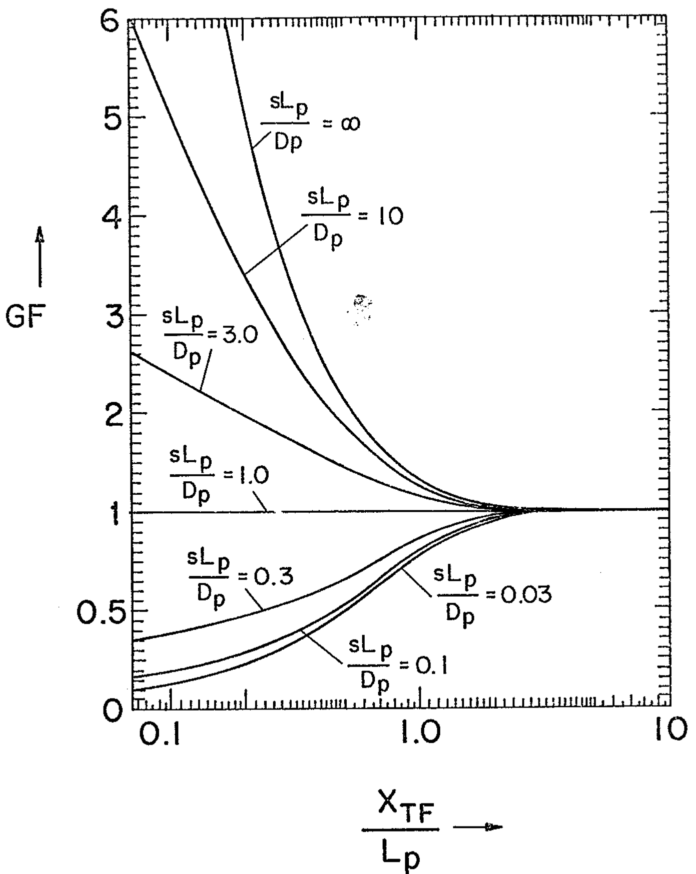

Figure 1

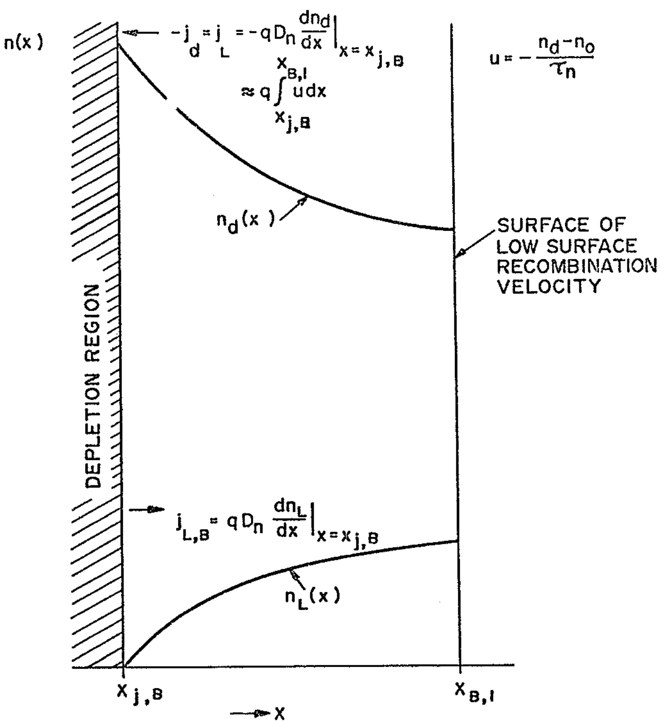

Figure 2

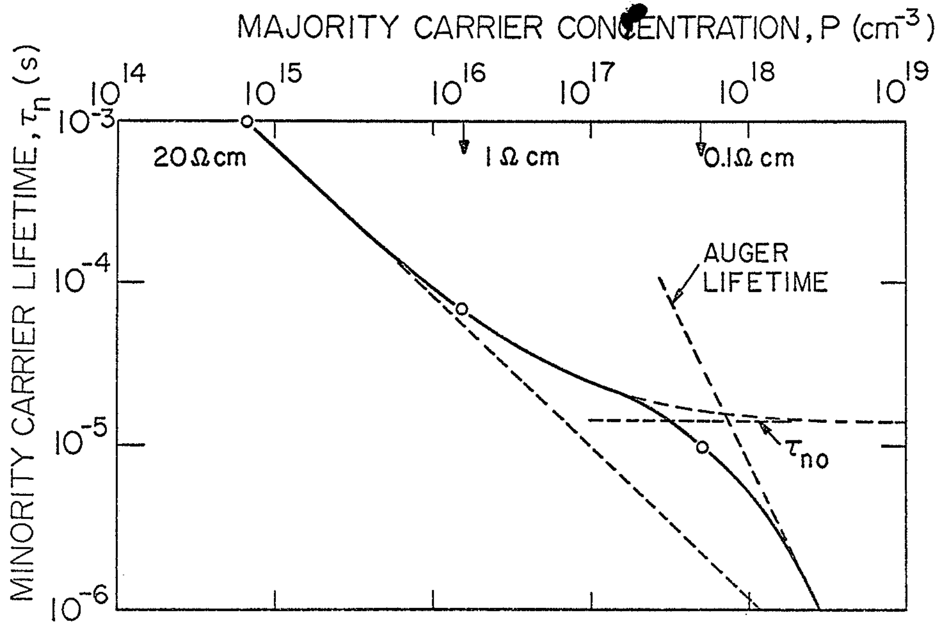

Figure 3

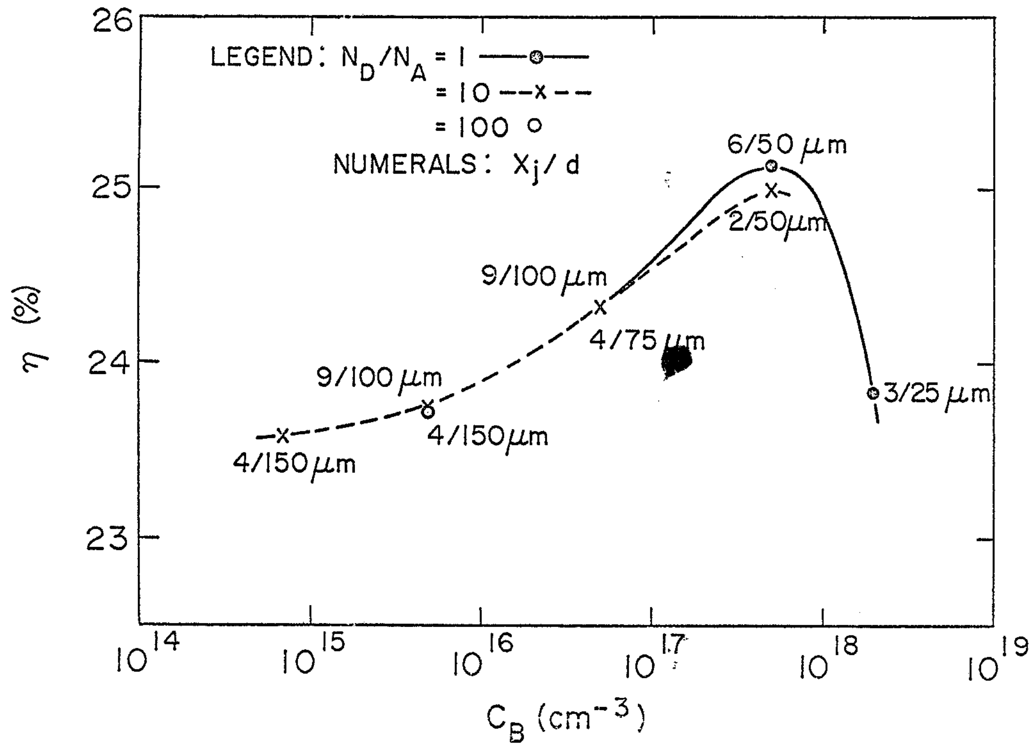

Figure 4

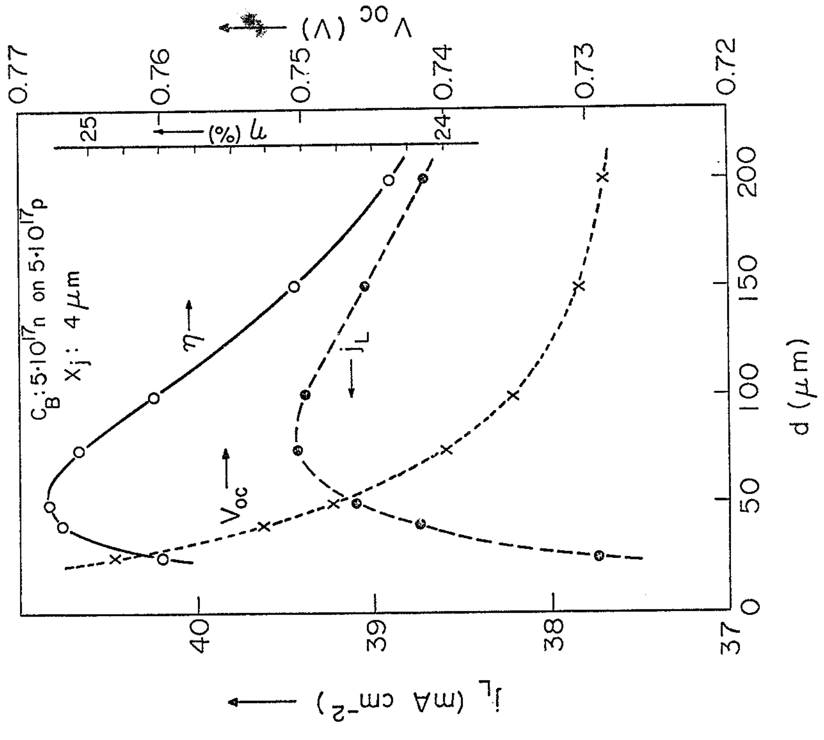

Figure 6

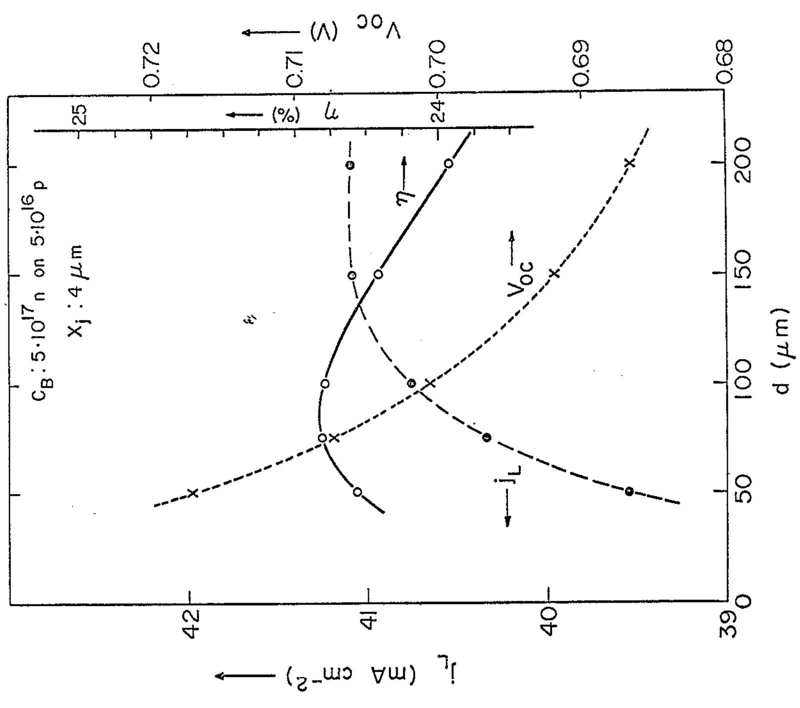

Figure 5

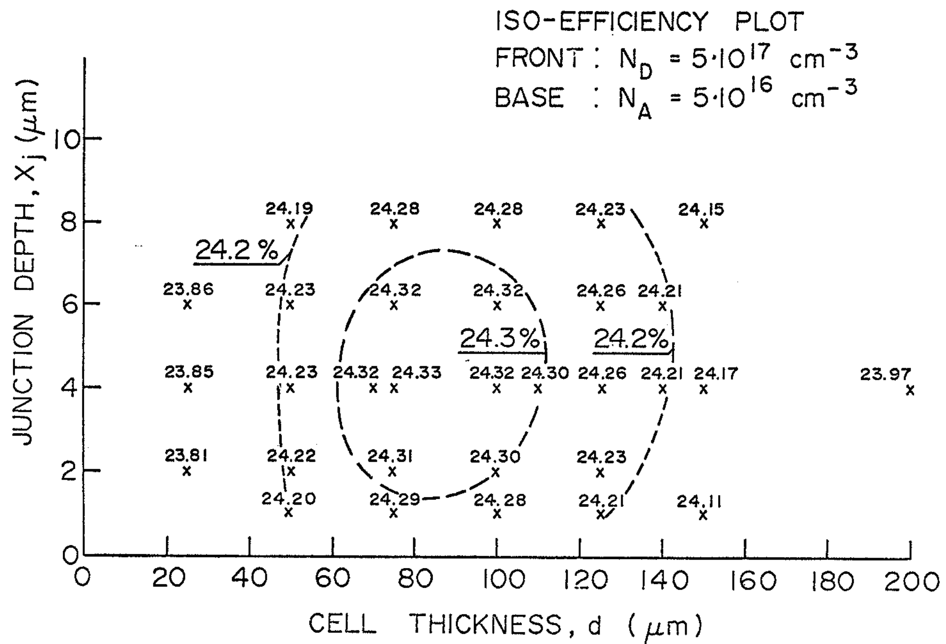

Figure 7

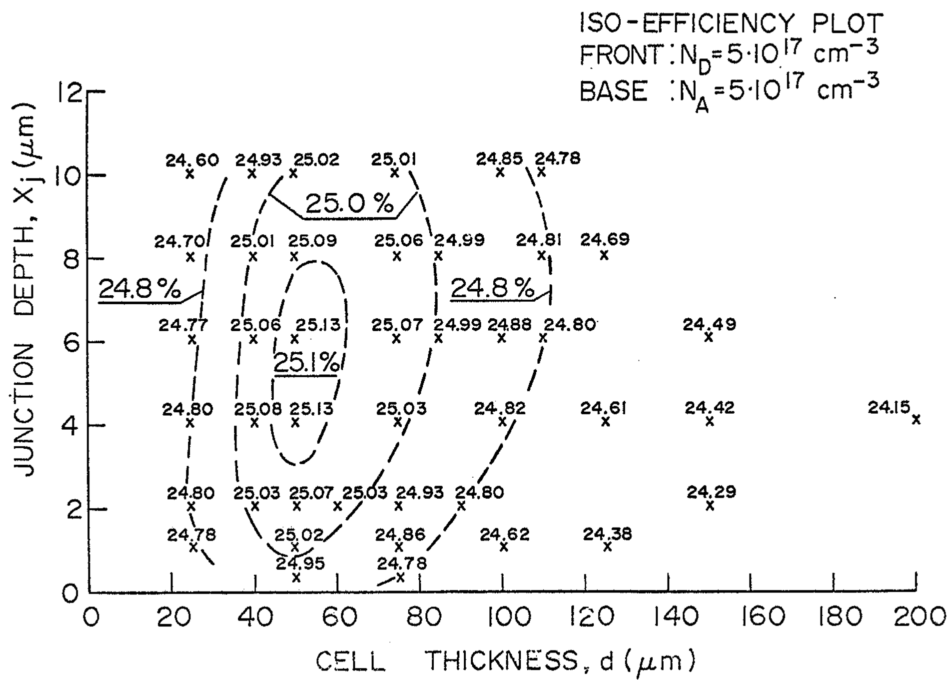

Figure 8